GEM TN-92-188

GEM Forward Calorimetry: A General Description of the Liquid Argon Option

John P. Rutherfoord
University of Arizona

September 25, 1992

Abstract:

The forward calorimeters for GEM are unique in that they will be located relatively close to the interaction point. This strategy has been examined in detail for a liquid argon technology using a new electrode structure of concentric tubes with narrow gaps. Following a general review of the requirements for GEM forward calorimetry is an overview of the liquid argon option.

GEM FORWARD CALORIMETRY
A GENERAL DESCRIPTION OF THE LIQUID ARGON OPTION

John Rutherfoord
University of Arizona

A general purpose detector for the SSC, which will attack the primary physics objectives of high p_T physics, must include in its capabilities a measurement of the missing E_T in each event. This requires that such a detector cover as much of 4π as possible so that no conventional particles are missed. The fiducial η coverage of the principal GEM detector elements is shown in Figure 1. The fiducial region for the forward calorimeters covers $3.0 \leq |\eta| \leq 5.0$ although their edges extend well beyond this range.

General physics topics which require forward calorimetry fall into two general classes, those which have missing E_T signatures and those which have jets at forward angles. These are listed in Figure 2.

The most demanding physics requirements on missing E_T come from potential SUSY signatures. For a perfect detector the principal background to the missing E_T signature is due to escaping neutrinos from heavy quark decay. The goal set by GEM is to design a detector which does not induce any significant additional background to this fundamental physics background.

The detailed Monte Carlo work of Paige and Vanyashian (GEM TN-92-70) has demonstrated that detector induced backgrounds are small compared to the irreducible neutrino background *if* there is full calorimeter coverage out to $|\eta|$ of at least 5.0 and *if* the E_T resolution for jets is 10% or better. So these are the design goals for GEM forward calorimetry. A SUSY signal with missing E_T above 100 GeV should be detectable at a luminosity at or below 10^{33} cm^{-2} sec^{-1}. In addition the forward calorimeter should be capable of dealing with luminosities in the range of 10^{34} cm^{-2} sec^{-1}. In this range missing E_T signatures in the 100 GeV region will have been explored and so higher values of missing E_T will be the target, say above 400 GeV.

There are two significant sources of detector induced backgrounds, 1) jet energy which escapes detection and 2) jets whose transverse energy is mismeasured.

For a well designed detector, the primary source of escaping jet energy is the beam hole, i.e. the region above $|\eta| = 5.0$ where it is impractical to provide coverage. But other sources include 1) cracks where tracker cables are brought out through the calorimeter, 2) structural members, 3) dead calorimeter channels, etc. These additional contributions can be minimized with proper design.

Sources of mismeasurement should be limited to angle and energy resolution effects in the calorimeters but cracks between displaced calorimeter elements can lead to hadronic shower leakage from one element to another and this energy flow cannot be distinguished from hadrons coming from the interaction region. This problem was first identified by the D0 group and is now known as the "η=3 crack" crossover problem. (A. Jonckheere, D0 Internal Note.)

These general considerations lead to the following performance requirements for the GEM forward calorimeters.

Coverage: As stated above, the forward calorimeters must make adequate measurements of the E_T of jets out to an $|\eta|$ of about 5.0.

Angle resolution and segmentation: In order to meet the design goal of $\Delta E_T/E_T \leq 10\%$ we must measure the angle of a jet with an accuracy of $\Delta\theta/\theta \leq 10\%$. This is a challenge, particularly at larger $|\eta|$ where θ is quite small. The transverse segmentation of the forward calorimeter must be fine enough to yield this angle resolution. Bins in $|\eta|$ of order 0.3 or smaller are adequate as long as intrinsic shower fluctuations don't dominate. Depth segmentation also aids angle resolution since the hadronic showers are tighter earlier in the shower process. Michael Shupe and J.P.R. (GEM TN 92-52) have shown that an optimal thickness for the first depth segment is approximately 2.5 λ. Finally a third depth segment allows one to tag late developing showers in order to flag the possibility that there is significant shower leakage out the back.

Energy resolution: In order to achieve an E_T resolution of 10% the energy resolution for jets must be somewhat better since the angle resolution, which is folded in quadrature with the energy resolution, is difficult to achieve. We estimate the energy resolution must be better than 6%. Jets with an E_T of order 100 GeV will have energy above 1 TeV. A calorimeter with a stochastic term smaller than $190\%/\sqrt{E}$ is probably adequate if the constant term is small. So due care is required to keep the constant term to of order 2%.

Calorimeter depth: For a missing E_T, a deep forward calorimeter is not necessary. While there might occasionally be a late developing shower which looses significant energy out of the end, this effect is second order compared to late developing showers in the region $|\eta| \leq 3$. But a deeper calorimeter may be necessary in order to shield the muon chambers. This is still under study.

Speed of response: To achieve adequate e/π in the forward calorimeter (in order to keep the constant term in the energy resolution small) the signal must be read out over a period of order 40 nsec. To avoid introducing any more physics pile-up noise than necessary the signal should be integrated in a time at least this fast. It is also important to identify the bunch crossing associated with the measured energy deposit. This is accomplished with a rise time shorter than the bunch spacing.

Radiation resistance: The forward calorimeter will be subjected to radiation levels which depend on the distance from the interaction region and on the luminosity. Figure 3 shows

the exposure of the calorimeter at EM shower max at a luminosity of 10^{34} cm^{-2} sec^{-1} for one SSC year for two choices of distance from the interaction point. Note that exposures of order 10 GRad per SSC year are expected at the larger values of $|\eta|$ in the forward calorimeter. Calorimeter materials which can withstand many years at these doses are required. Further the performance of the calorimeter must not degrade with time. It will already be a challenge to achieve the performance requirements with no exposure.

Radiation to other detector elements: Neutron albedo in the central tracker volume is a problem for the performance of the tracking devices. The forward calorimeter should not contribute a significant fraction of this neutron flux. Leakage of charged and neutral particles into the muon system is also a problem. The GEM muon group is developing requirements which the forward calorimeter must meet.

Activation: The calorimeter will become quite radioactive during a run. While this radioactivity will die away with time, it must be possible for personnel access to nearby detector elements without undue radiation exposure. Access to the insides of the forward calorimeter itself is problematic.

In the face of these general requirements the SDC collaboration and the LHC experiments have opted for forward calorimeters located as far from the interaction point as possible. The GEM collaboration has explored a different optimization. Figure 4 shows the liquid argon option with the forward calorimeter at the right. Nested with the endcap, the forward calorimeter should be a source of less spray into the muon system than in the other detectors. The "$\eta = 3$ crack" problem is reduced because the lever arm that allows spray to cross over the beam line is reduced. And the cost is lower because the volume of calorimeter is greatly reduced and services are shared. On the other hand we must deal with higher densities of ionizing radiation and fluxes of neutrons. And the geometry of showers and jets is different. For instance, for even the densest of calorimeters, the transverse hadronic shower size in the calorimeter is larger than the typical jet cone size of 0.7 in $\eta - \phi$ space.

The forward calorimeter is, in most respects, a conventional sampling, ionization, liquid argon calorimeter in that it collects charge from ionizing shower fragments in the sensitive medium, the liquid argon. At ultra high rates such calorimeters suffer some degradation due to the distortion of the electric field which collects the charge. This distortion is due to the accumulation of positive argon ions which drift out to the electrodes more slowly than the electrons. This effect has been calculated in detail (J. Rutherfoord, GEM TN-91-27) and the effect on the signal is shown on Figure 5. The signal is not degraded until the background ionization rate reaches a critical value (r=1 in Figure 5) where the accumulated positive ions equal the charge on the electrodes. This critical ionization rate depends inversely on the square of the electrode separation for a constant electric field. To avoid this problem, even at 10^{34} cm^{-2} sec^{-1}, we have chosen an electrode separation in the EM segment of 100 μm. In the hadronic segments the electrode separation is 300 μm.

It is not easy to maintain the tolerance on such gaps in the conventional parallel plate

calorimeter so we have employed a "tube" design. An exploded view of a single tube electrode is shown in Figure 6. Experience with such tube electrodes is reported in GEM TN-92-179.

These tubes are arranged in an hexagonal array as shown in Figure 7. Dimensions are tabulated in Figure 8. The tubes are parallel to the beam line and their diameters and separations increase from module to module in proportion to the distance of the module from the interaction point. This provides a *pseudo projective* arrangement which allows a simple construction with adequate transverse segmentation and good angle resolution. The three modules are shown in greater detail in Figure 9. Figure 10 is a distorted view of one tube in the "EM" module at $\eta = 4.5$. The vertical scale is greatly expanded relative to the horizontal in order to evaluate potential channeling effects. The ray from the interaction point suggests that the aspect ratio of the gap in these tubes is small enough that channeling effects will be small.

A front view of the EM module is shown in Figure 11. As described earlier the transverse and depth segmentation are both chosen to optimize the angle resolution. Figure 12 is at the same scale as Figure 11 and can be overlaid on it. Shown are the sizes of electromagnetic and hadronic showers in this forward calorimeter and jets at various values of η. Note that a jet at $\eta = 5.0$ is appreciably smaller than a hadronic shower. Figure 13 is a close-up of the front face of the EM module in the region of the beam pipe showing the segmentation and the tube electrodes by circles only.

Detailed simulation at two different levels has been carried out on this design (M. Shupe, GEM TN-92-xxx and P. Loch, GEM TN-92-xxx). The summary plot showing the E_T resolution versus η for 200 GeV hadrons is shown in Figure 14. The calorimeter which was simulated in GEANT is as described here with the segmentation shown in Figure 11. Different beam hole sizes are shown. Statistics are still accumulating so this plot will have less scatter at a later time. Right now the statistical precision can be seen particularly for the points at $\eta = 4.8$ where the data should show progressively poorer resolutions as the beam hole radius increases. Since jet cone sizes are smaller than the lateral size of hadronic showers at the larger values of $|\eta|$ we believe that simulating single hadrons is sufficient for many of our studies.

As shown in Figure 8 the total drift time for the charge in the EM module is 20 nsec while in the hadronic modules it is 60 nsec. Just as in the barrel and endcaps this signal will be shaped to give an effective integration time of 30 nsec. For the EM module this will result in almost no ballistic deficit. Any calorimeter will have a pre-sample in order to estimate the baseline and this must be added to the sampling time. We conservatively estimate a total integration time of 3 bunch crossings.

If hadronic showers had no transverse spreading then the physics pile-up noise in a given $\Delta\eta \times \Delta\phi$ tower would be roughly independent of η and would increase with the square root of the luminosity. A reasonable tower size to choose is a jet cone which is also independent of η for QCD jets. However hadronic showers do spread and at $\eta = 5$ they spread over

an area which is somewhat larger than a jet cone. However Eric Stern (GEM TN-92-111 and to be submitted to NIM) has shown that while the pile-up increases due to shower spreading, the fluctuations actually decrease since more showers are contributing less E_T in a given tower. So physics pile-up noise in a jet cone is smaller than it is at smaller $|\eta|$. Ignoring shower spreading the physics pile-up noise in a jet cone of radius 0.7 and for an integration time of three bunch crossings is 1.1 GeV in E_T. This will increase by about a factor 3 at 10^{34} cm^{-2} sec^{-1}.

The electronics noise in the same jet cone radius measured in E_T is about 0.9 GeV at $|\eta| = 4$. It decreases at larger $|\eta|$.

The physics pile-up noise and electronics noise each contribute to the E_T resolution quadratically in the $1/E$ term. So at an E_T of 100 GeV and at 10^{33} cm^{-2} sec^{-1} they contribute 1.1% and 0.9% respectively, entirely negligible amounts.

The signals from the tubes will be ganged at each module and then brought out of the calorimeter on low impedance striplines to common base "line terminators" (see S.Rescia *et al.*, Submitted to NIM) located at the outer radius of the endcap calorimeter. So no forward calorimeter electronics will be subjected to any irradiation. This electronics scheme, called the "zero transistor solution", makes optimal use of the transmission line properties of the stripline so that the risetime of the signal is barely degraded for fairly long signal paths. It is ideally suited to our forward calorimeter where speed of signal is at a premium and where the electronics cannot be situated locally.

The large flux of particles from min bias events, particularly near the beam pipe, deposit heat in the forward calorimeters. An appreciable quantity of heat actually comes, not directly from the ionization in the absorbers, but from ohmic heating of the drifting ions in the liquid argon gaps. At 10^{34} cm^{-2} sec^{-1} this heating is about 100 watts in the EM module and 200 watts in the hadronic modules. The density of heat deposition is large in the EM section where most is concentrated about the beam pipe near EM shower maximum. The heat is conducted away primarily by the Tungsten absorber material. The actual heat conduction calculation is quite difficult for our complicated geometry but a worst case approximation designed to bracket the problem gives a temperature difference between the "hot" spot and the module outer radius, where liquid nitrogen cooling loops will be located, of less than 1 Kelvin, a most acceptable temperature gradient. Heat transport from the liquid argon to the absorber material gives rise to much smaller temperature differences due to the small gaps.

Radiation damage is a real concern for our forward calorimeters at such close distances to the interaction point. Doses in excess of 10 GigaRad in one SSC year at 10^{34} cm^{-2} sec^{-1} will be experienced in the regions close to the beam pipe. (These doses will pale in comparison to those received by the collimators which protect the final focus quads a short distance away.) The liquid argon design will be carefully engineered to use no materials which are susceptible to radiation damage. The sensitive material, i.e. the liquid argon, is not at all affected by ionizing radiation other than by the creation of ions which

drift in the electric field and are neutralized at the electrodes. (The positive ion buildup problem was discussed above.) The absorber material is also highly radiation resistant. The very few additional materials which will be in the cryostat will also be carefully chosen to avoid radiation damage. The quartz fibers with kapton cladding were mentioned above. The optical properties of the quartz are not a concern to us. Copper conductors, G10 insulators, solder, and kapton dielectrics round out the list of construction materials so far identified. When the forward calorimeter technology is chosen a detailed R&D program will be conducted to test each material under massive doses.

Activation calculations are in progress. So far Laurie Waters estimates that the radiation levels for the hottest portions of the forward calorimeter, when opened up, will be about 140 mR on contact after one SSC year at 10^{33} cm^{-2} sec^{-1} and then after one day of "cool down". These hot spots will be near the beam pipe and will be well shielded by the rest of the forward calorimeter. She is now in the process of estimating the personnel dose to a worker at some distance from the fully assembled forward calorimeter.

The design of the liquid argon option has been stable for some time and has allowed us to study it in considerable detail. We have a reasonable level of confidence that the design is feasible and will meet our physics goals. Choice of the liquid argon option would not be unreasonable at this time. A complete R&D program for the next year is mapped out and we are eager to get on with it.

Figure Captions

1) Fiducial coverage of major GEM detector elements. The hadronic calorimeter systems include the forward calorimeters which blanket the region $3.0 \leq \eta \leq 5.0$.

2) A listing of physics processes which require forward calorimetry.

3) Radiation exposure to a calorimeter in Grays (1 Gy = 100 Rad) at EM shower max for two different distances from the interaction point in one SSC year.

4) Quarter section of the GEM calorimeter, liquid argon option. The interaction point is at the lower left and the beam line runs along the bottom. The forward calorimeter is at the right.

5) The signal from a single gap of a liquid argon calorimeter as a function of the rate of background ionization in the gap. The signal, S, is relative to the signal at zero background ionization rate. A background ionization rate, r, of unity corresponds to that rate where the charge due to positive ions builds up to a level which equals the charge on the electrodes necessary to maintain the electric field in the liquid argon.

6) An exploded view of a tube electrode. The inner rod is Tungsten absorber and is held at a potential of about 100 volts. The outer tube is stainless steel and is held at ground.

Outside the outer tube is Tungsten absorber, not shown. A kapton clad quartz fiber is spiraled about the inner rod to maintain the gap.

7) Hexagonal arrangement of tube electrodes in the forward calorimeter absorber. The round shaded region represents a Tungsten inner rod. The very thin ring represents the volume occupied by liquid argon. The slightly wider ring outside this represents a stainless steel tube. The six-sided shaded piece represents one "pellet" of Tungsten absorber.

8) Table of parameters for the liquid argon design.

9) Cross section in the plane of the beam of the GEM liquid argon forward calorimeter.

10) Longitudinal cut of one tube in the "EM" module at $\eta = 4.5$ on a scale which is 50×1 vertical to horizontal. A superposed ray from the interaction point (IP) crosses the liquid argon gap at a "steep" angle.

11) The segmentation of the front face of the "EM" section of the GEM forward calorimeter, liquid argon option. The scale on the left is in meters while the scale on the right is in η with demarkations at segmentation breaks.

12) On the same scale as Figure 11 are shown the sizes of EM and hadronic showers. For the hadronic showers "Radial" means that fraction of a shower contained within a cylinder of the size shown while "Lateral" means that fraction of a shower contained in a strip of the width shown. The latter is useful at boundaries. Also shown are the sizes of jet cones of $\Delta R = 0.7$. Note that jets at $\eta = 5$ are appreciably smaller than hadronic showers in this calorimeter.

13) Close-up view of the front face of the EM module in the region of the beam pipe. The segmentation is indicated. The tube electrodes are indicated by the small circles.

14) E_T resolution ($\Delta E_T/E_T$) versus η for the segmentation shown in Figure 10. The data are generated via GEANT using 200 GeV charged pions. Different sizes of the beam hole are shown. At press time the statistics of the simulation were limited and this shows particularly for the points at $\eta = 4.8$.

GEM Coverage

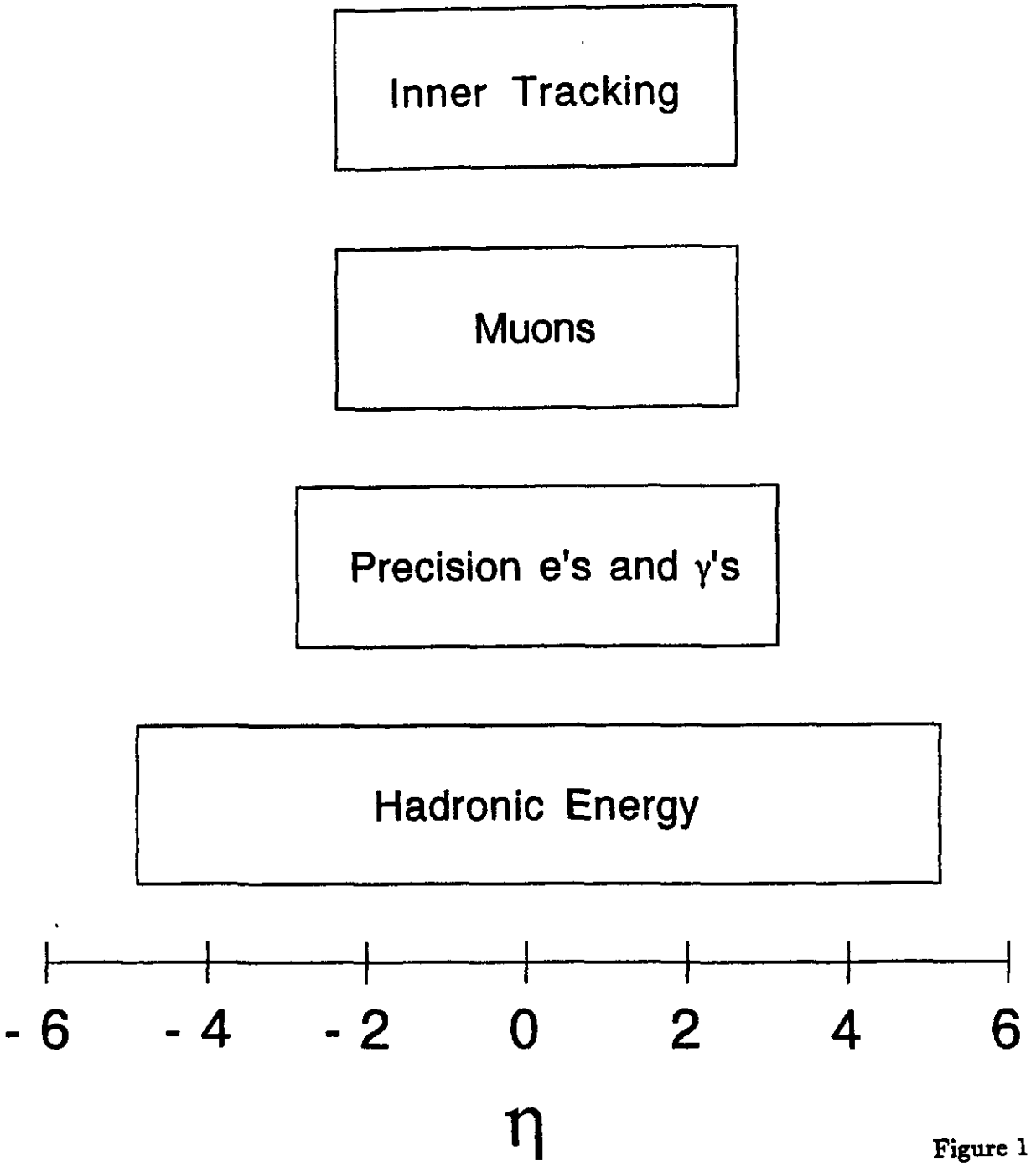

Figure 1

Physics Requiring a Forward Calorimeter

Missing E_T

Higgs

$$H \rightarrow ZZ \rightarrow \ell^+\ell^-\nu\bar{\nu}$$
$$H \rightarrow ZZ \rightarrow \ell^+\ell^-\tau\bar{\tau}$$

New heavy quarks

SUSY

Technicolor

$$\rho_{TC}^{\pm} \rightarrow W^{\pm}Z^o \rightarrow \ell^{\pm}\nu\ell^+\ell^-$$
Leptoquarks $gg \rightarrow P_3P_3 \rightarrow b\tau\bar{b}\bar{\tau}$

New Gauge Bosons

$$W'^{\pm} \rightarrow \ell^{\pm}\nu$$

Other sources of boson pairs

$$W^{\pm}Z^o \rightarrow \ell^{\pm}\nu\ell^+\ell^-$$
$$W^{\pm}W^{\pm} \rightarrow \ell^{\pm}\nu\ell^{\pm}\nu$$
$W^+W^- \rightarrow \ell^+\nu\ell^-\nu$ if separable from $t\bar{t}$

Forward Jets

VV scattering with forward jet tagging

Low x physics via forward di-jets

Figure 2

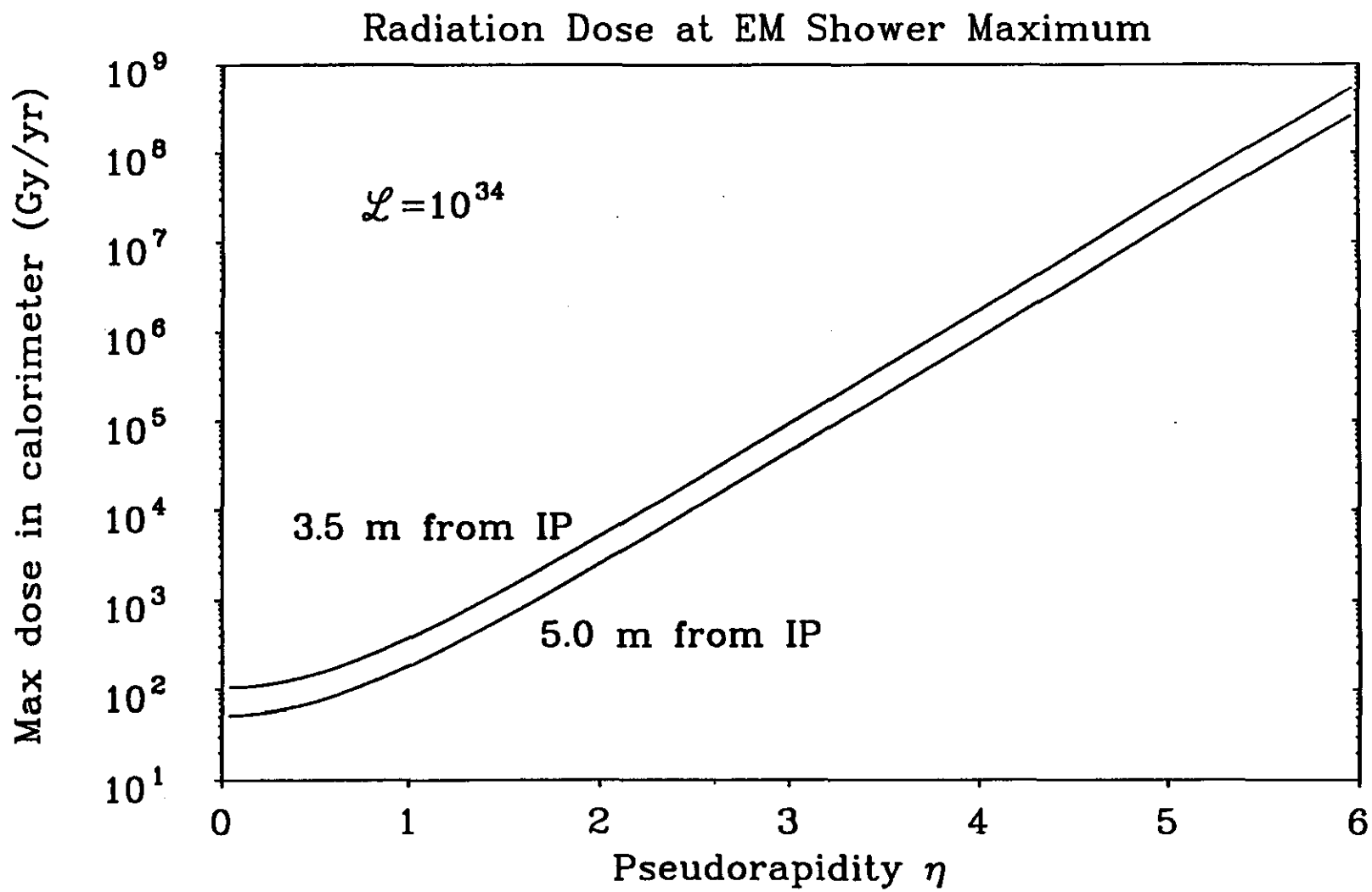
Radiation Dose at EM Shower Maximum
Max dose in calorimeter (Gy/yr)
10^9
10^8
10^7
10^6
10^5
10^4
10^3
10^2
10^1
$\mathcal{L}=10^{34}$
3.5 m from IP
5.0 m from IP
0
1
2
3
4
5
6
Pseudorapidity η

Figure 3

LIQUID ARGON CALORIMETER - 12 X 14 LAMBDA, FLAT ENDCAP HEAD

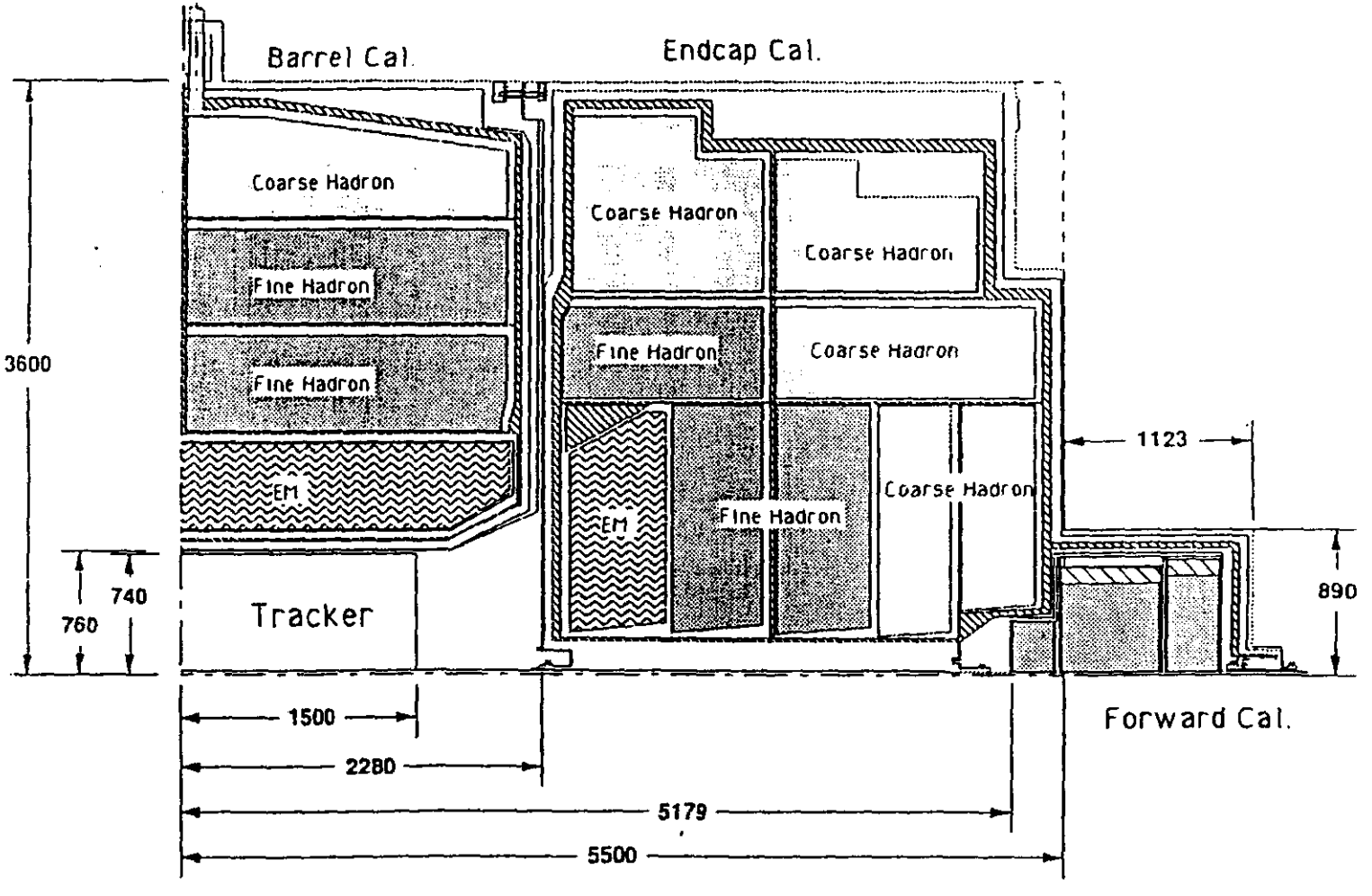

Figure 4

Dimensions in millimeters

LLMASON 920620 5A55 .DL

004

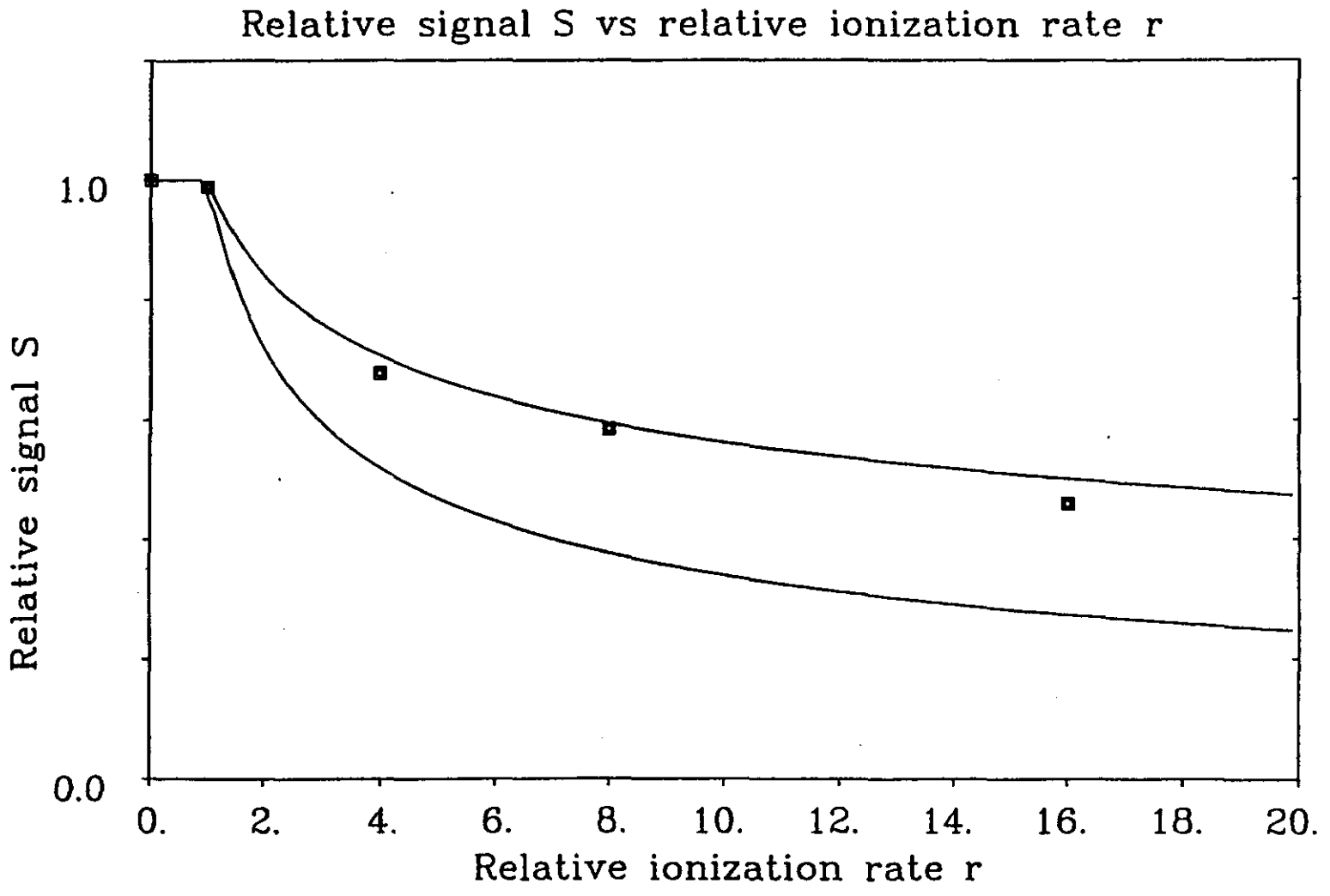
Relative signal S vs relative ionization rate r
1.0
0.0
Relative signal S
0.
2.
4.
6.
8.
10.
12.
14.
16.
18.
20.
Relative ionization rate r

Figure 5

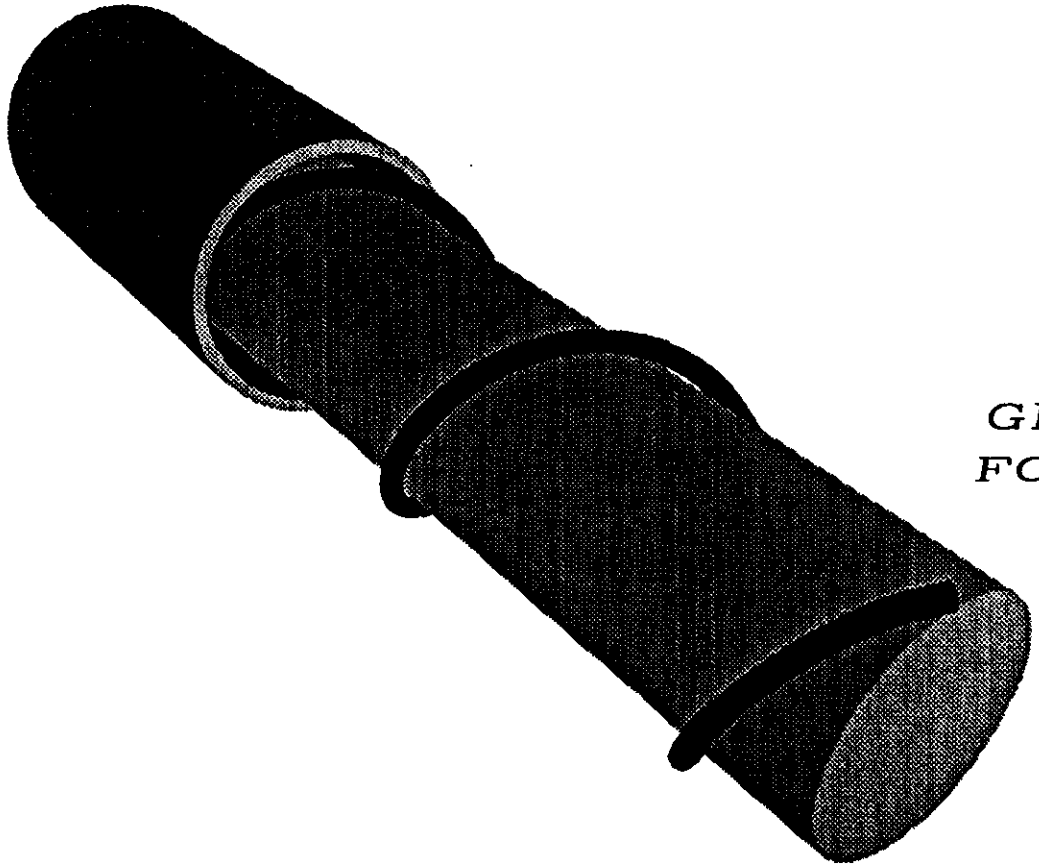

GEM LAC
FCal Tube

Figure 6

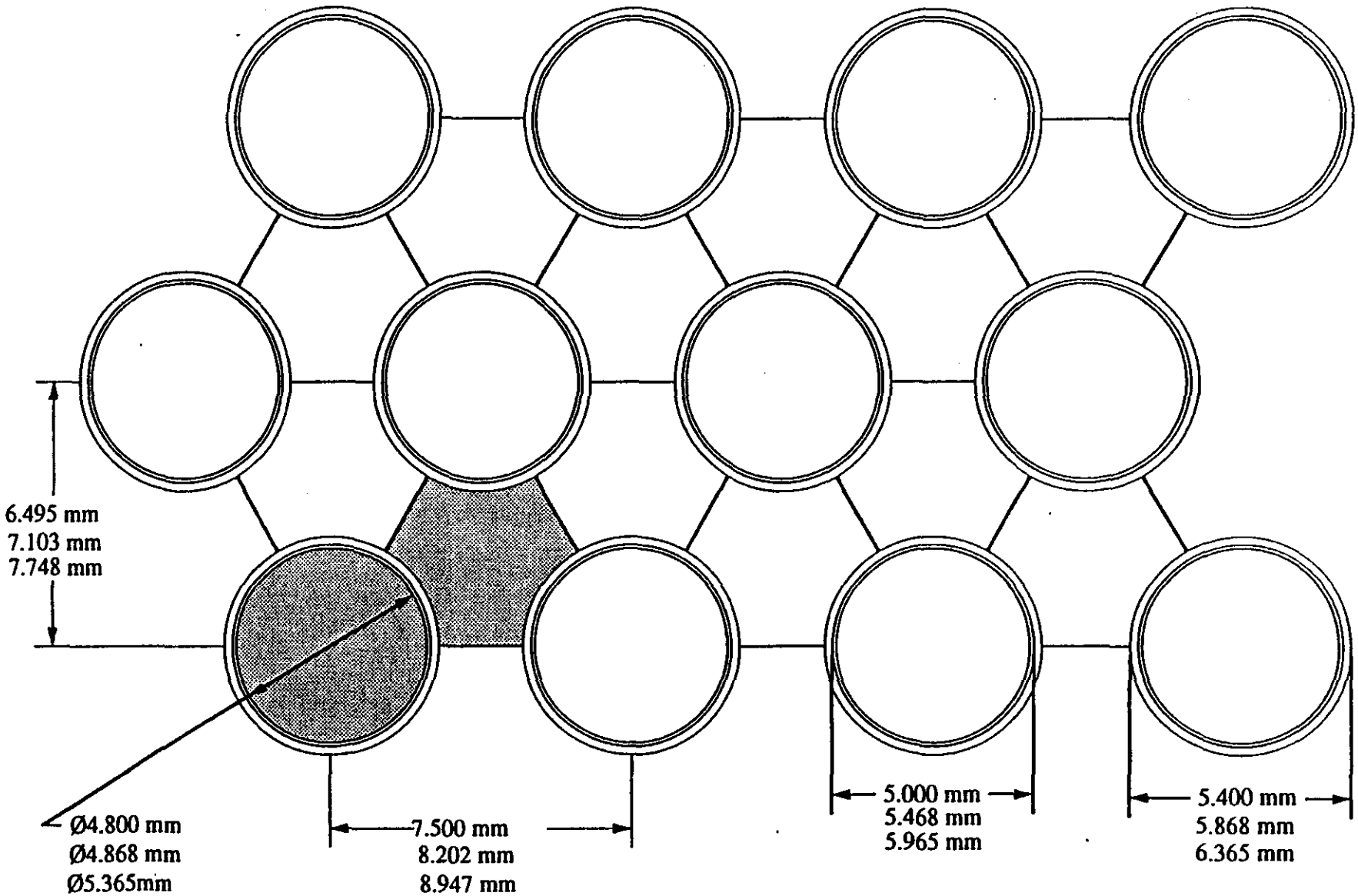

Figure 7

FCAL MODULE - TUNGSTEN ARRAGEMENT

GEM FCal Detailed Parameters

Parameter/Module	1	2	3
Name	"EM"	Hadronic Tail Catcher	
Distance from IP to near face (mm)	5090.00*	5385.00	6005.00
Depth in z (mm)	250.00*	570.00*	300.00*
Dist from IP to module mid-plane (mm)	5215.00	5670.00	6155.00
Inner radius (mm)	20.00*	21.74	23.60
Outer radius (mm)	330.00*	566.00*	614.00
Unit Cell			
Center-to-center tube separation (mm)	7.50*	8.15	8.85
Tube diameter ID (mm)	5.00*	5.44	5.90
Tube wall thickness (mm)	0.20*	0.20*	0.20*
Tube OD/2 (mm)	2.70	2.92	3.15
LAr gap (mm)	0.10*	0.30*	0.30*
Voltage across gap (V)	125.00	375.00	375.00
Drift time (nsec)	20.00	60.00	60.00
Cross sectional area of			
Unit cell (mm^2)	48.71	57.59	67.86
Heavymet (mm^2)	43.91	49.20	58.75
Tube (mm^2)	3.27	3.54	3.83
Gap (mm^2)	1.54	4.84	5.28
Average density (g/cm^3)	17.01	16.19	16.34
Sampling fraction (%)	0.34	0.94	0.86
Interaction Length (mm)	105.34	110.48	109.56
Tube capacitance (pF)	544.87	433.63	248.93
Tube inductance (nH)	2.04	13.33	6.43
Tube impedance (Ohms)	1.94	5.54	5.08
Weight (metric tonnes)	1.45	9.27	5.80
Area of mod less tube OD/2 at each edge	0.33	0.99	1.17
Number of tubes	6875.35	17264.28	17241.83
Towers evenly divided into eta-phi bins			
5.4<eta<6.2			
eta bins	1.00	1.00	1.00
phi bins	12.00	6.00	6.00
4.8<eta<5.4			
eta bins	2.00	1.00	1.00
phi bins	20.00	10.00	10.00
4.2<eta<4.8			
eta bins	4.00	2.00	2.00
phi bins	32.00	16.00	16.00
3.4<eta<4.2			
eta bins	6.00	3.00	3.00
phi bins	48.00	24.00	24.00
3.0<eta<3.4			
eta bins	0.00	2.00	2.00
phi bins	0.00	40.00	40.00

Figure 8

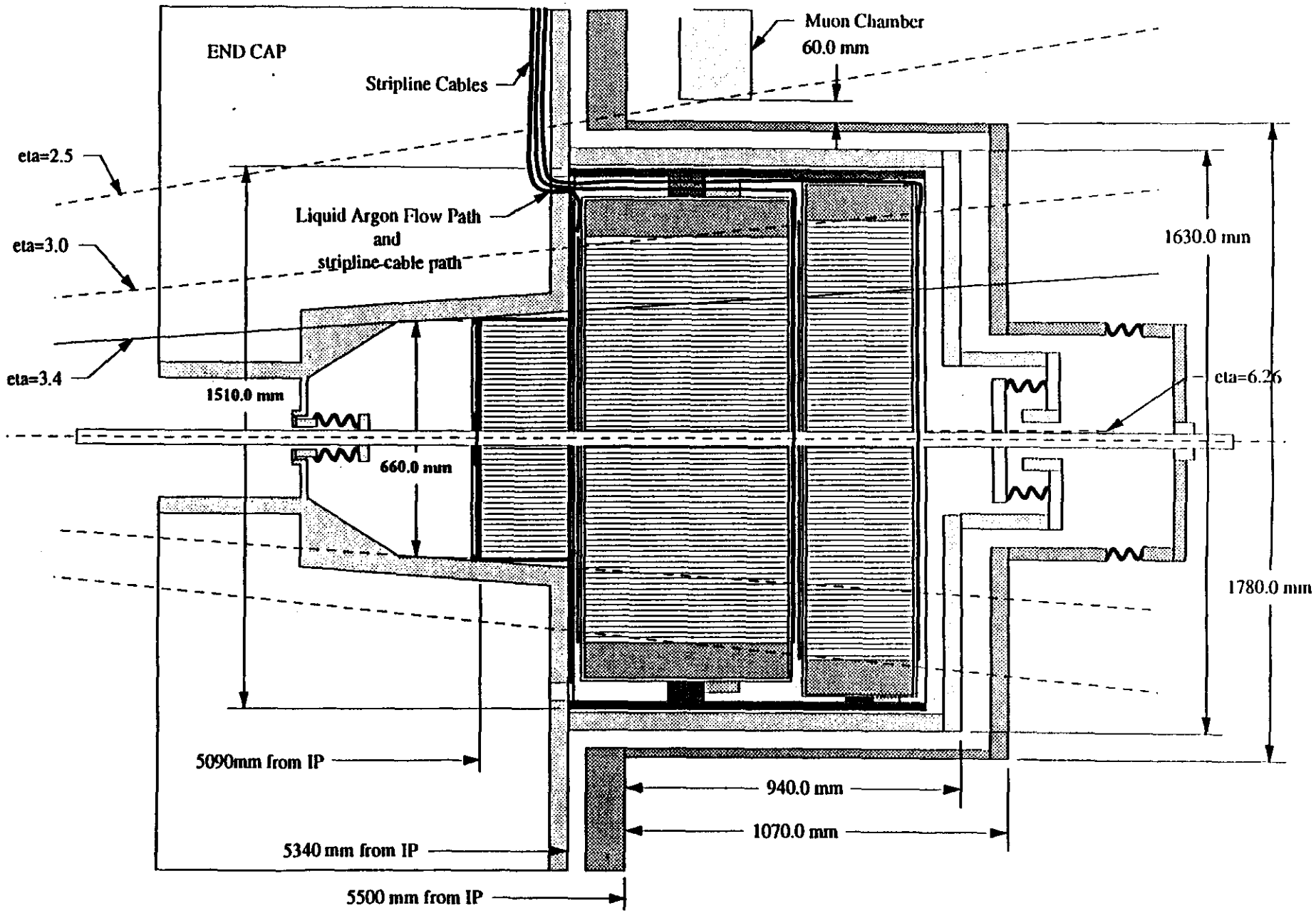

FORWARD CALORIMETER
LIQUID ARGON OPTION
GENERAL ARRANGEMENT

Figure 9

FCLAR-GA001

S. M. CHAE

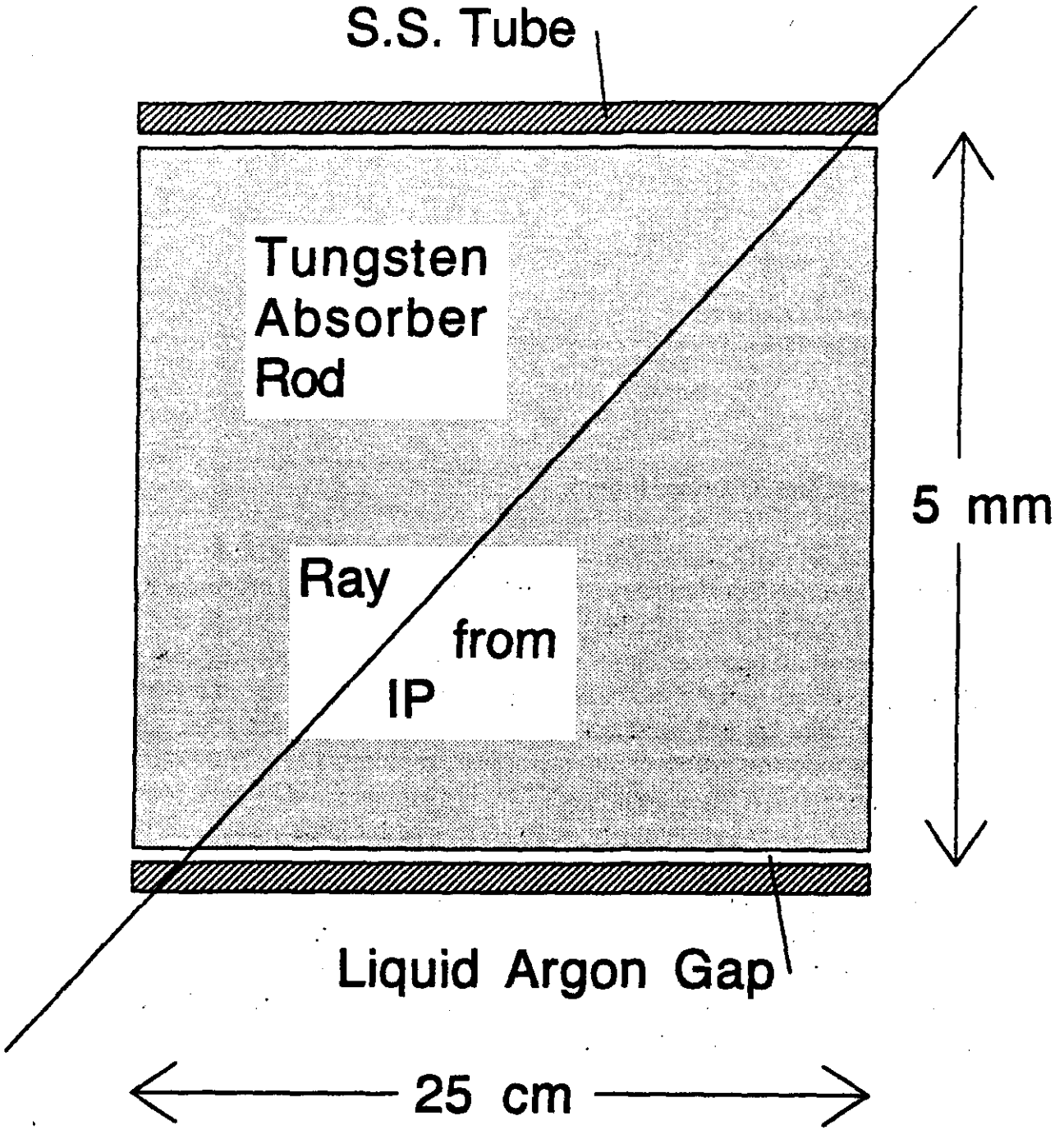
S.S. Tube
Tungsten
Absorber
Rod
Ray
from
IP
5 mm
Liquid Argon Gap
25 cm

Figure 10

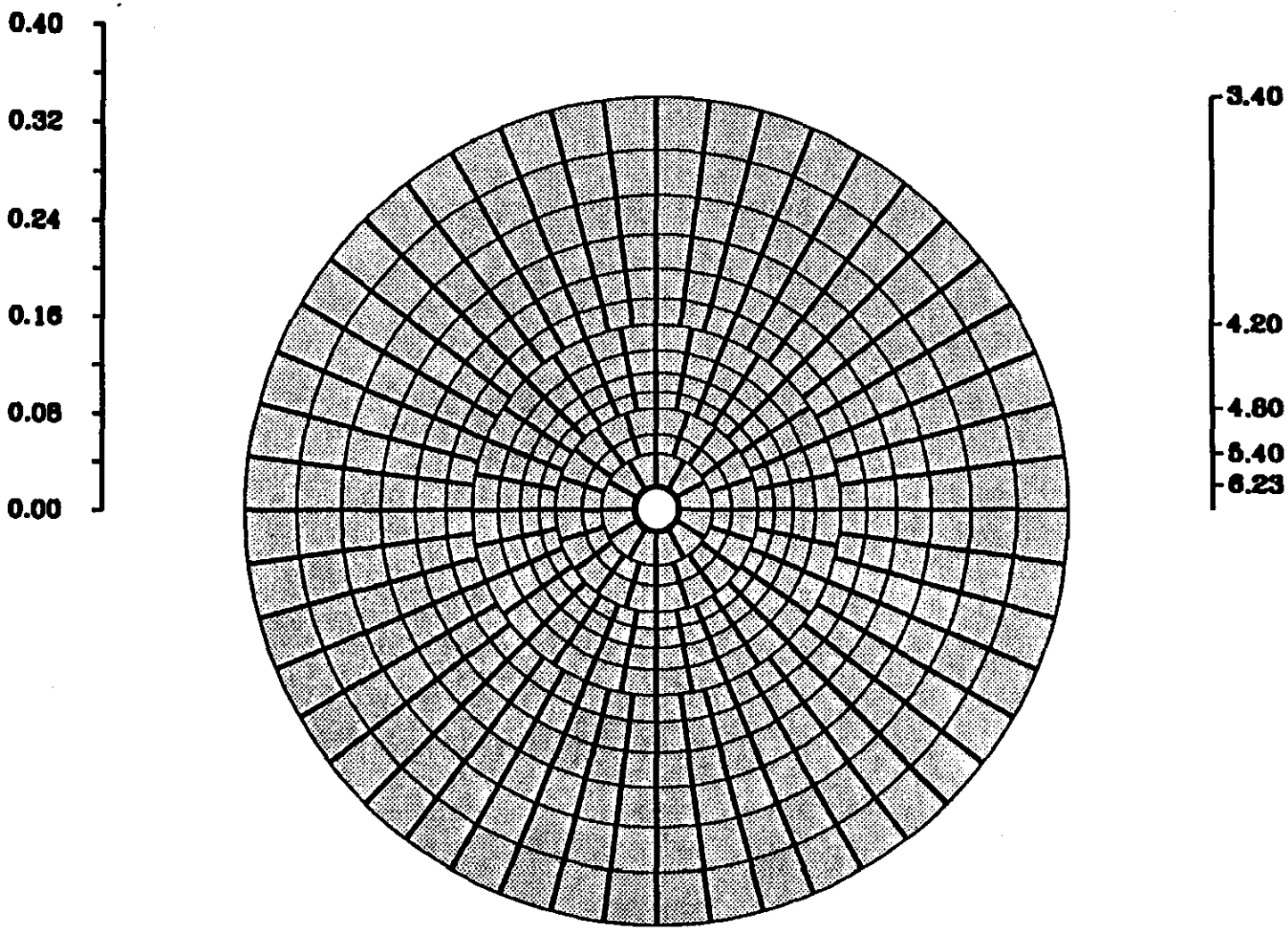

Figure 11

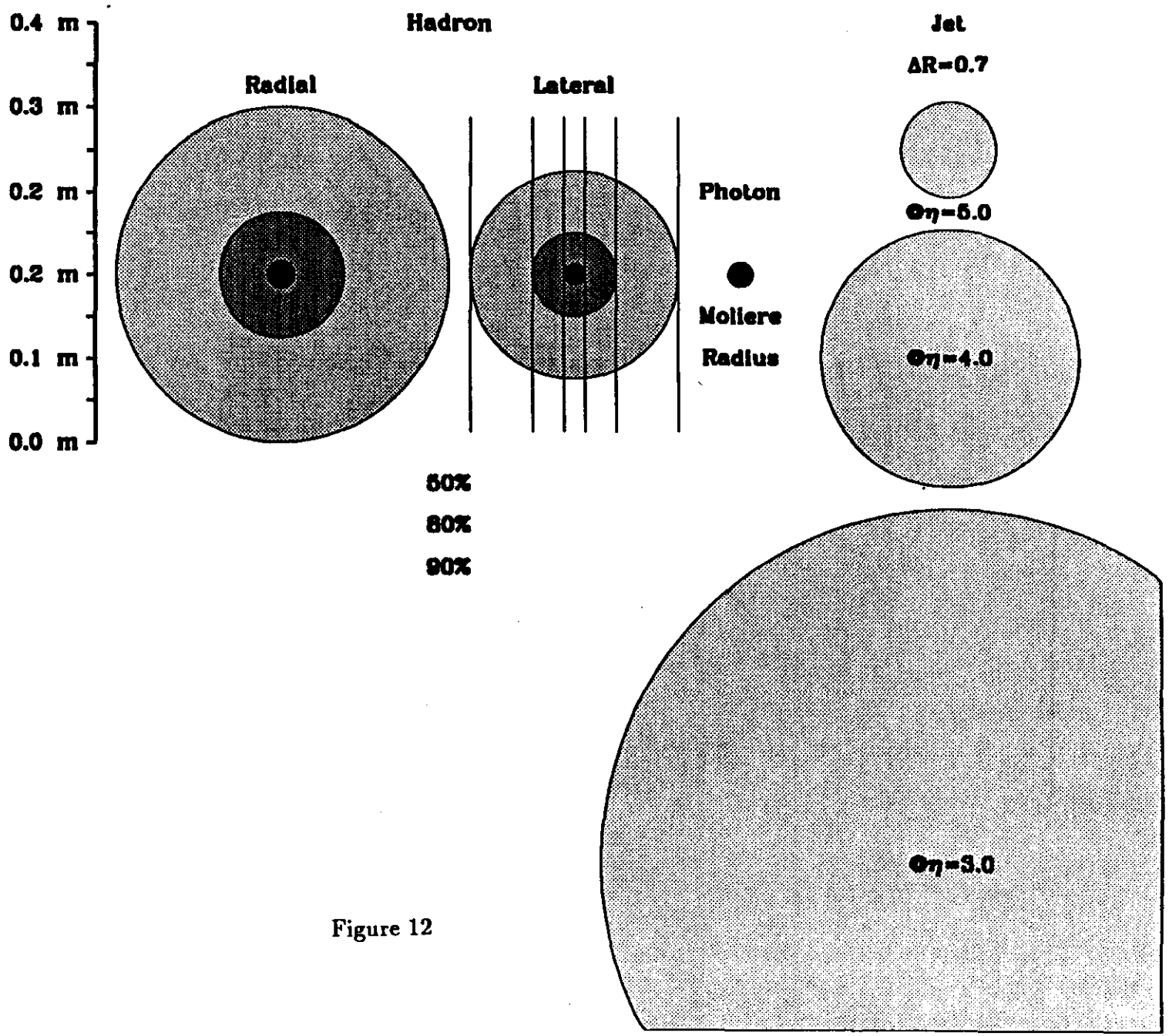
0.4 m
0.3 m
0.2 m
0.2 m
0.1 m
0.0 m
Hadron
Radial
Lateral
Photon
Moliere
Radius
50%
80%
90%
Jet
ΔR=0.7
Φη=5.0
Φη=4.0
Φη=3.0

Figure 12

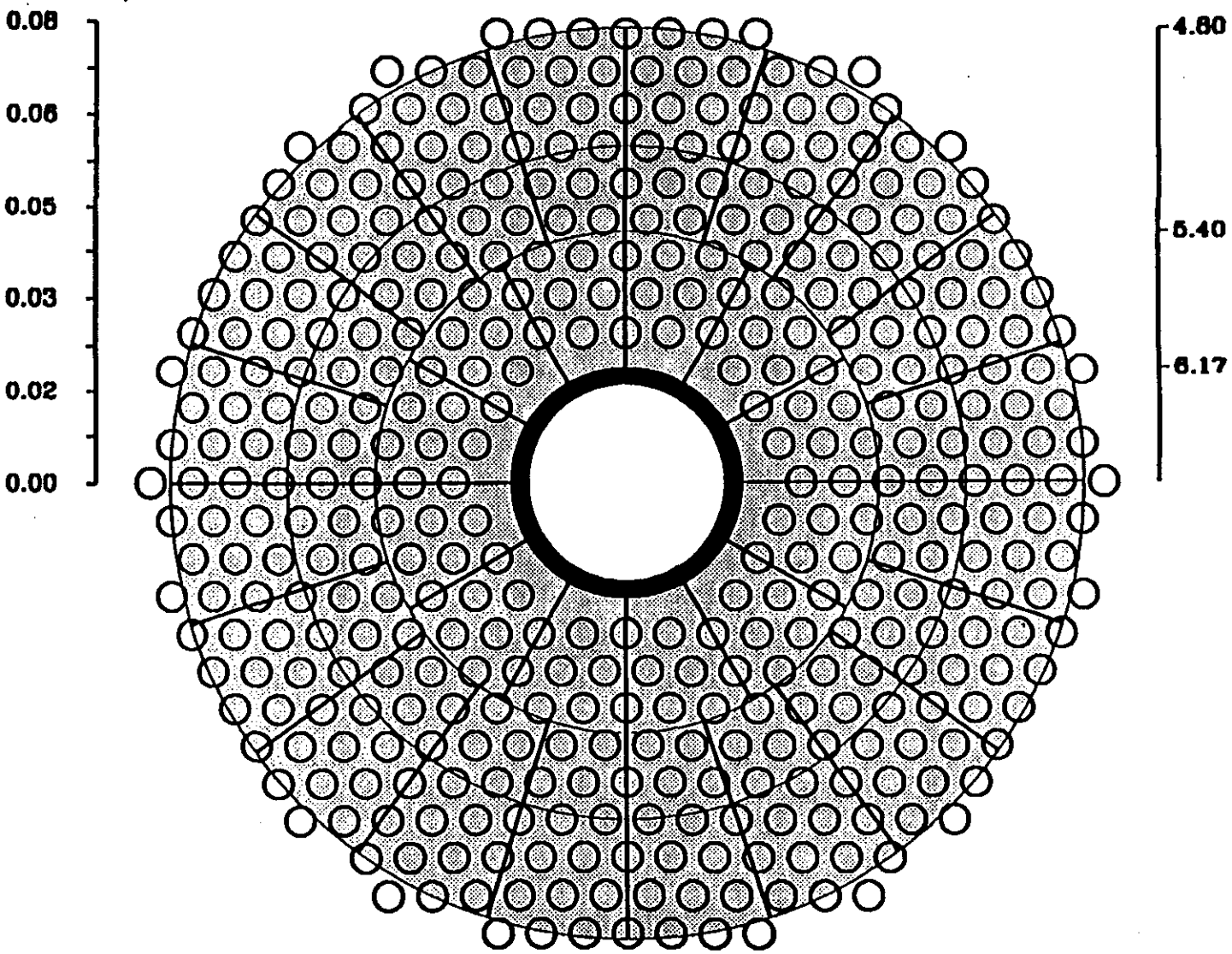

Figure 13

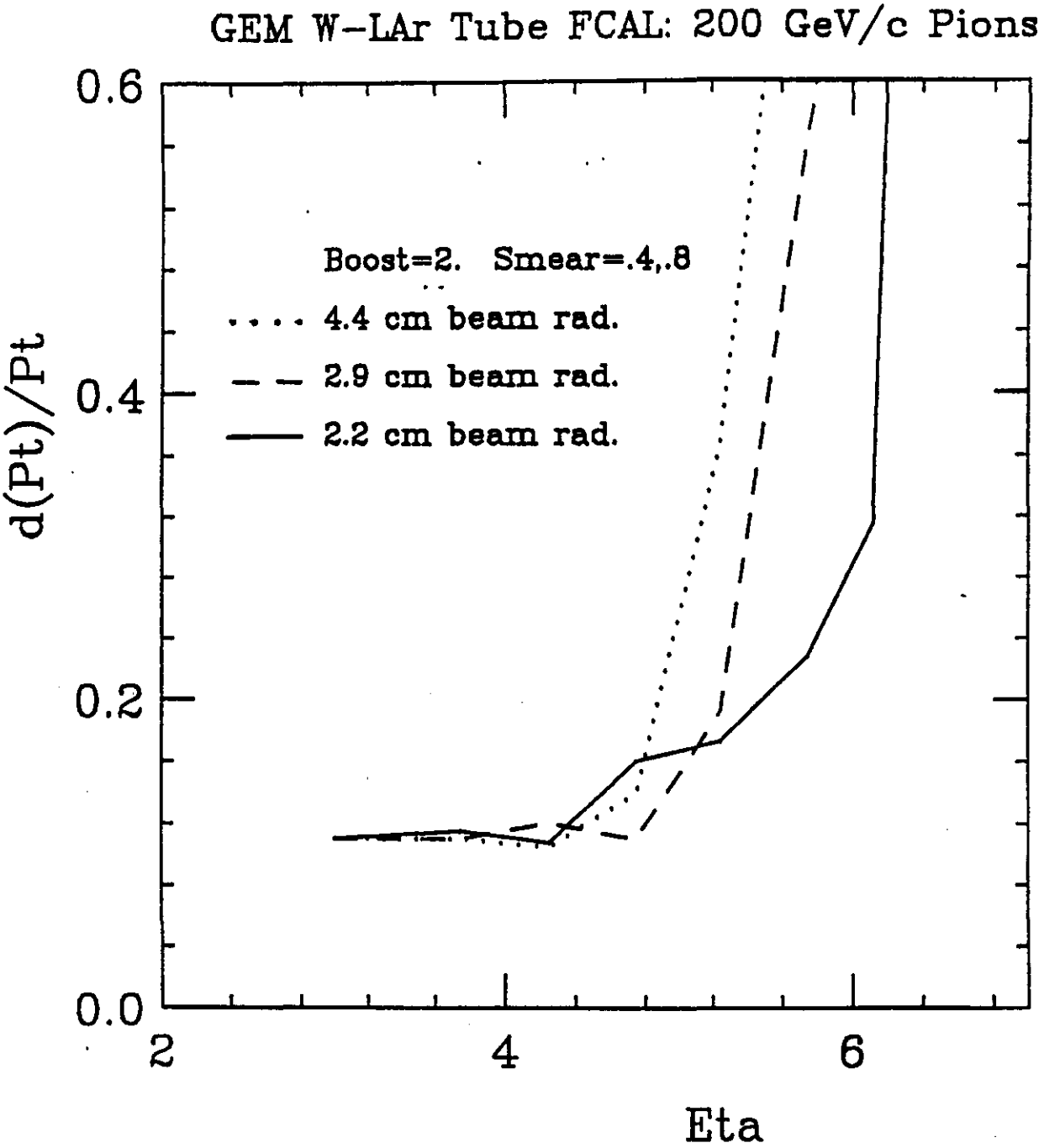
GEM W-LAr Tube FCAL: 200 GeV/c Pions
Boost=2. Smear=.4,.8
4.4 cm beam rad.
2.9 cm beam rad.
2.2 cm beam rad.
d(Pt)/Pt
0.0
0.2
0.4
0.6
2
4
6
Eta

Figure 14